PCCP

Accepted Manuscript

This is an *Accepted Manuscript*, which has been through the Royal Society of Chemistry peer review process and has been accepted for publication.

Accepted Manuscripts are published online shortly after acceptance, before technical editing, formatting and proof reading. Using this free service, authors can make their results available to the community, in citable form, before we publish the edited article. We will replace this *Accepted Manuscript* with the edited and formatted *Advance Article* as soon as it is available.

You can find more information about *Accepted Manuscripts* in the **Information for Authors**.

Please note that technical editing may introduce minor changes to the text and/or graphics, which may alter content. The journal's standard **Terms & Conditions** and the **Ethical guidelines** still apply. In no event shall the Royal Society of Chemistry be held responsible for any errors or omissions in this *Accepted Manuscript* or any consequences arising from the use of any information it contains.

Alcohol-Soluble Interfacial Fluorenes for Inverted Polymer Solar Cells: Sequence Induced Spatial Conformation Consequently Dipole Moment

Lie Chen[a,b], Xiangfu Liu[a], Yingkai Wei[a], Feiyan Wu[a], Yiwang Chen*[a,b]

[a]College of Chemistry/Institute of Polymers, Nanchang University, 999 Xuefu Avenue, Nanchang 330031, China

[b]Jiangxi Provincial Key Laboratory of New Energy Chemistry, Nanchang University, 999 Xuefu Avenue, Nanchang 330031, China

Corresponding author. Tel.: +86 791 83968703; fax: +86 791 83969561. E-mail: ywchen@ncu.edu.cn (Y. Chen)

Lie Chen and Xiangfu Liu contributed equally to this work.

1

Abstract:

Three fluorene-based alcohol-soluble organic small molecule electrolytes (SMEs) with different conjugated backbones, namely, TFTN-Br, FTFN-Br, and FTTFN-Br were designed as cathode interfacial layers for inverted polymer solar cells (i-PSCs). Insertion of SMEs to ITO/active layer interfaces effectively lowered the energy barrier for electron transport, and improved the inherent compatibility between the hydrophilic ITO and hydrophobic active layers. Due to these advantages, the device based on poly (3-hexylthiophene) (P3HT):(6,6)-phenyl-C_{61} butyric acid methyl ester ($PC_{61}BM$) with TFTN-Br as cathode interfacial layers achieved an improved power conversion efficiency (PCE) of 3.8%, which is 26% improvement compared to the standard device with ZnO cathode interfacial layers (PCE=3.0%). Devices with FTFN-Br and FTTFN-Br also showed the improved PCE of 3.1% and 3.5%, respectively. The variation of device performance enhancement is found to be primarily correlated with the different the conformation of their assembly onto the electrode caused by the joint sequence of polar group of SMEs, consequently impacting the dipole moment and interface morphology. In addition, introducing SMEs as cathode interfacial layers also brought the devices with long-term stability.

Keywords: Electrolytes; Interfacial layers; Dipole moment; Polymer solar cells

Introduction

Bulk heterojunction (BHJ) polymer solar cells (PSCs) blending of conjugated polymers and fullerene acceptors have attracted abundant attention for their potential advantages, such as low cost, mechanical flexible, lightweight and easy fabrication for large-area production.[1-3] Recently, single-junction PSCs have already broken a power conversion efficiency (PCE) record of 10%.[4, 5] Usually, there are two main device configurations: the conventional and the inverted structures. And it has been come to realized that the inverted device structure is superior over the conventional device structure.[6-9] On account of the acid poly(3,4-ethyl-enedioxythiophene):(polystyrene sulfonic acid) (PEDOT:PSS) anode and the easily oxidized low work function cathode metals in conventional device,[10, 11] the inverted devices have testified much better device stability with metal oxide (ZnO or TiO_x) as the bottom cathode and employed the high work function metals (Cu or Ag) as the top anode. Furthermore, the inverted structure make good use of the vertical composition gradient in active layer, with fullerene-rich phase approach the cathode and polymer-rich phase approach the anode.[12-15] The key issue in inverted PSCs is to develop an interfacial materials to tune the energy alignment and improve the contact interface between the photoactive layer and ITO cathode,[16, 17] which can promote the charge selective transport and collection.

Currently, a variety of electron-transporting layer (ETL) materials have been applied in the inverted PSCs, including inorganic metal oxides (such as Cs_2CO_3, TiO_x and ZnO) and organic materials (such as PFN, PEIE).[18-23] The inorganic interfacial materials can give an decent device performance,[24] however, the compatible processing temperatures of the metal oxides with temperature sensitive substrates for organic electronics is a perplexed issue for the researcher.[25] Moreover, these inorganic materials have the poor interfacial contact with the organic active layer. Thus, organic materials are often incorporated as interfacial layer to modulate or replace inorganic materials. These organic interlayers, including conjugated polymer electrolytes (CPEs) and small molecule electrolytes (SMEs), have been drawn more and more attention

for excellent modification on the electrode. Compared to the CPEs, the SMEs are easy purification, monodispersity, well-defined structures and better batch-to-batch reproducibility. Although SMEs has rendered the device with notable effieciency,[26] the exploration of the SMEs interlayers for PSCs is still rare, and lag much behind the CPEs interlayers.

Taking the advantages of the SMEs into account, in this paper, three fluorene-based alcohol-soluble small molecular electrolytes (SMEs) with different conjugated backbones, 6-(2,7-bis(5-octylthiophen-2-yl)-9-(6-(trimethy lammonio) hexyl)-9H-fluoren-9-yl)-N,N,N-trimethylhexan-1-aminium bromide (**TFTN-Br**), 6-(2-(5-(9,9-bis(6-(trimethylammonio)hexyl)-9H-fluoren-2-yl)thiophen-2-yl)-9-(6-(tri methylammonio)hexyl)-9H-fluoren-9-yl)-N,N,N-trimethylhexan-1-aminium bromide (**FTFN-Br**),6-(2-(5-(5-(9,9-bis(6-(trimethylammonio)hexyl)-9H-fluoren-2-yl)thiophn -2-yl)thiophen-2-yl)-9-(6-(trimethylammonio)hexyl)-9H-fluoren-9-yl)-N,N,N-trimeth ylhexan-1-aminium bromide (**FTTFN-Br**), bearing amine groups on side chains, are designed and synthesized. These SMEs are well soluble in methanol (MeOH), dimethyl formamide (DMF), dimethylsulfoxide (DMSO) and other polar solvents, but show poor solubility in the nonpolar solvents such as chlorobenzene (**Figure S1** in Supporting Information (SI)), which can avoid the erosion from the upper organic active layer in the inverted polymer solar cells (i-PSCs),[27] and favor the environment friendly process as well. It can be found that the conjugated backbone of the SMEs influenced greatly on the conformation of their assembly onto the electrode, consequently impacting the dipole moment and interface morphology. Compared to FTFN-Br and FTTFN-Br, TFTN-Br can provide more compatible contact between ITO and active layer, improve charge mobility and achieve a better energy alignment in the device. The device based on poly (3-hexylthiophene) (P3HT):(6,6)-phenyl-C$_{61}$ butyric acid methyl ester (PC$_{61}$BM) with TFTN-Br as ETL achieves an improved power conversion efficiency (PCE) of 3.8%, which is 26% improvement compared to the standard device with ZnO ETL (PCE=3.0%). Devices with FTFN-Br and FTTFN-Br ETL also showed the improved PCE of 3.1% and 3.5%, respectively.

Experimental Section

The details of general measurements and characterization are shown in Supporting Information.

The synthesis of the SMEs:

2-Bromo-9, 9-bis(6-bromohexyl)-9H-fluorene (1)

To a solution of 2-bromo-9H-fluorene (2.0 g, 8.2 mmol, 1 equiv) in tetrahydrofuran (THF) (60 mL), was added KOH (1.00 g) and H_2O (5 ml). After being stirred for 2 h, the 6-dibromohexane (2.50 g, 3.28 mmol, 2.5 equiv) was added dropwised and then kept at room temperature for overnight. Then the solution was poured into brine and extracted with ethyl ether twice, which was combined and dried over sodium sulfate. The solvent was removed and the crude product was subjected to silica gel chromatography (n-hexane) to give the product (1) (3.75 g, 80%). ^{1}H-NMR(CDCl$_3$, 400 MHz): δ (ppm) 7.67 (m, 1H), 7.56 (m, 1H), 7.46(dd, 2H), 7.33 (m, 3H), 3.28 (t, 4H), 1.95 (m, 4H), 1.64 (m, 4H), 1.18 (dt, 4H), 1.08 (dd, 4H), 0.59 (m, 4H).

2,5-Bis(9,9-bis(6-bromohexyl)-9H-fluoren-2-yl)thiophene (2)

The (1) (2.0 g, 3.5 mmol, 2 equiv), Pd(PPh$_3$)$_4$ (100 mg), and 2,5-bis(trimethylstannyl)thiophene (0.75 g, 1.7 mmol, 1 equiv) were weighed into a 100 mL round-bottom flask. The flask was vacuumed and protected with N_2 and then toluene (30 mL) was added. The reaction was carried out at 110 °C for 24 h, after which the solution was diluted with dichloromethane. The solvent was removed and the crude product was purified through chromatography on silica gel with hexanes to give the product (2) (2.23 g, 60%) as yellow solid. ^{1}H-NMR(CDCl$_3$, 400 MHz): δ (ppm) 7.72 (d, 4H), 7.67 (d, 2H), 7.61 (s, 2H), 7.40 (d, 2H), 7.33 (m, 6H), 3.28 (t, 8H), 2.04 (t, 8H), 1.66 (m, 8H), 1.20 (dd, 8H), 1.10 (dt, 8H), 0.68 (m, 8H).

2-(9,9-Bis(6-bromohexyl)-9H-fluoren-2-yl)-5-(5-(9,9-bis(6-bromohexyl)-9H-fluoren-2-yl)thiophen-2-yl)thiophene(3)

The synthesis of (3) from (1) was similar to the procedure of (2) from (1), and the 2,5-bis(trimethylstannyl)thiophene was replaced by 2-(trimethylstannyl)-5-(5-

(trimethylstannyl)thiophen-2-yl)thiophene, giving yellow solid in 70% yield. ^{1}H-NMR (CDCl$_3$, 400 MHz): δ (ppm) 7.70 (d, 4H), 7.61 (d, 2H), 7.54 (s, 2H), 7.33 (m, 8H), 7.23 (d, 2H), 3.27 (t, 8H), 2.01 (t, 8H), 1.64 (dd, 8H), 1.19 (m, 8H), 1.10 (m, 8H), 0.65 (m, 8H).

6-(2-(5-(9,9-Bis(6-(trimethylammonio)hexyl)-9H-fluoren-2-yl)thiophen-2-yl)-9-(6-(trimethylammonio)hexyl)-9H-fluoren-9-yl)-N,N,N-trimethylhexan-1-aminium bromide (FTFN-Br)

Condensed trimethylamine (5.0 mL) was added dropwised to a solution of (2) (0.2 g) in tetrahydrofuran (25 mL) at 0 $^\circ$C. The mixture was allowed to warm up to room temperature gradually. The precipitate was redissolved by addition of excess water and an extra 2 mL trimethylamine was added at 0 $^\circ$C. The resulting mixture was stirred for 24 h at room temperature and the yellow precipitate was collected by filtration. After purified by recrystallization from chloroform and hexane and dried in a vacuum oven to give as a yellow solid (0.18 g, 95%). ^{1}H-NMR(DMSO, 400 MHz): δ (ppm) 7.84 (m, 6H), 7.68 (m, 4H), 7.45 (s, 2H), 7.33 (d, 4H), 3.11 (m, 8H), 2.93 (s, 36H), 2.43 (s, 8H), 2.05 (t, 8H), 1.43 (m, 8H), 1.03 (m, 16H), 0.55 (m, 8H). ^{13}C-NMR(DMSO, 400 MHz): δ (ppm) 152.66, 151.78, 144.98, 142.52, 142.20, 134.61, 128.60, 128.37, 125.75, 125.62, 124.10, 121.45, 120.95, 120.66, 67.74, 49.33, 49.19, 49.04, 48.90, 48.76, 48.62, 30.16, 26.81, 24.67, 23.58.

6-(2-(5-(5-(9,9-Bis(6-(trimethylammonio)hexyl)-9H-fluoren-2-yl)thiophen-2-yl)t-hiophen-2-yl)-9-(6-(trimethylammonio)hexyl)-9H-fluoren-9-yl)-N,N,N-trimethylh exan-1-aminium bromide (FTTFN-Br)

The synthesis of **FTTFN-Br** from (3) was similar to the procedure of **FTFN-Br** from (2), giving yellow solid in 95% yield. ^{1}H-NMR (DMSO, 400 MHz): δ (ppm) 7.81 (m, 6H), 7.65 (m, 4H), 7.44 (m, 4H), 7.33 (m, 4H), 3.12 (m, 8H), 2.94(s, 36H), 2.03 (t, 8H), 1.42 (m, 9H), 1.03 (m, 17H), 0.52 (m, 9H). ^{13}C-NMR(DMSO, 400 MHz): δ (ppm) 151.56, 150.68, 143.26, 141.01, 140.55, 135.89, 125.79, 124.85, 123.41,

121.19, 119.87, 65.61, 55.29, 52.54, 40.47, 40.33, 40.20, 40.06, 39.92, 39.78, 39.64, 39.30, 29.15, 25.88, 23.81, 22.38.

Tributyl(5-octylthiophen-2-yl)stannane (4)

A solution of 2-octylthiophene (5.0 g, 25.5 mmol, 1 equiv) in anhydrous THF (100 mL) was degassed through argon for 15 min and then a n-BuLi solution (2.4 M in hexanes, 11.7 mL, 1.1 equiv) was added at -78 °C dropwised. The resulting solution was kept at -78 °C for 10 min and then room temperature for 2 h. After dropping of tributylchlorostannane (9.1g, 28.05 mmol, 1.1 equiv) at -78 °C, it was kept at room temperature for overnight. Then the solution was poured into brine and extracted with ethyl ether twice, which was combined and dried over sodium sulfate. The solvent was removed and the crude product was subjected to silica gel chromatography (n-hexane) to give (4) as colorless oil (7.5 g, 75%). ^{1}H-NMR(CDCl$_3$, 400 MHz): δ (ppm) 7.01 (d, 1H), 6.93 (d, 1H), 2.88 (t, 2H), 1.63 (m, 8H), 1.33 (m, 15H), 1.10 (m, 4H), 0.93 (m, 12H).

2-(9,9-Bis(6-bromohexyl)-7-(5-octylthiophen-2-yl)-9H-fluoren-2-yl)-5-octylthiophene (5)

The synthesis of (5) from 2,7-dibromo-9,9-bis(6-bromohexyl)-9H-fluorene was similar to the procedure of (2) from (1), giving yellow solid in 80% yield. ^{1}H-NMR(CDCl$_3$, 400 MHz): δ (ppm) 7.67 (d, 2H), 7.56 (m, 4H), 7.23 (d, 2H), 6.80 (d, 2H), 3.27 (t, 4H), 2.85 (t, 4H), 2.03 (t, 4H), 1.75 (m, 4H), 1.66 (m, 4H), 1.43 (m, 4H), 1.31 (m, 20H), 1.20 (m, 4H), 0.92 (m, 6H), 0.70 (m, 4H).

6-(2,7-Bis(5-octylthiophen-2-yl)-9-(6-(trimethylammonio)hexyl)-9H-fluoren-9-yl) -N,N,N-trimethylhexan-1-aminium bromide (TFTN-Br)

The synthesis of **TFTN-Br** from (5) was similar to the procedure of **FTFN-Br** from (2), giving yellow solid in 95% yield. ^{1}H-NMR(CD$_3$OD, 400 MHz): δ (ppm) 7.67 (d,

2H), 7.62 (s, 2H), 7.55 (d, 2H), 7.28(d, 2H), 6.80 (d, 2H), 3.12 (m, 4H), 2.96 (d, 18H), 2.83 (t, 4H), 2.12 (m, 4H), 1.72 (m, 4H), 1.48 (m, 4H), 1.35 (m, 20H), 1.13 (s, 8H), 0.89 (m, 6H), 0.65 (m, 4H). ^{13}C-NMR(CD$_3$OD, 400 MHz): δ (ppm) 151.28, 145.40, 119.12, 66.38, 48.13, 47.98, 47.84, 47.70, 47.56, 47.42, 47.28, 31.73, 31.63, 29.15, 29.08, 28.87, 22.42,13.1，141.91, 140.08, 133.85, 125.32, 124.28, 122.66, 119.99.

Device Fabrication: Polymeric solar cells were fabricated based on poly (3-hexylthiophene) (P3HT): (6, 6)-phenyl-C$_{61}$ butyric acid methyl ester (PC$_{61}$BM) with ZnO or SMEs as electron transport layers (ETLs). All devices were fabricated on pre-treatment ITO glass substrates, cleaned sequentially using sonication in acetone, detergent, deionized water, isopropanol and then dried under a nitrogen stream, followed by ultraviolet light irradiation. The ZnO precursor solution which was prepared according to the previous literature reported.[19] The methanol solution of SMEs with a concentration of 0.5 mg mL^{-1} was then spin coated at 3000 rpm for 30 s onto the ITO substrate. Whereafter, the active layer of P3HT:PC$_{61}$BM (1:0.8 w/w) in 1,2-dichlorobenzene was spin coated, followed by thermal annealing at 150 $^{\circ}$C for 10 minutes in the glovebox. Eventually, the double-layer structure of molybdenum trioxide (MoO$_3$) (7 nm)/argentum (Ag) (90 nm) was deposited over the active layer by thermal evaporation under a vacuum of 6 × 10^{-4} Torr to accomplish the device fabrication. The effective area of one cell was 0.04 cm^2. The *J-V* curves were measured with a Keithley 2400 source meter (100 mW/cm^2, AM 1.5 G, Abet Solar Simulator Sun2000). The IPCE spectra were detected on an IPCE measuring system (Oriel Cornerstone 260 1/4 m monochromator equipped with Oriel 70613NS QTH lamp). All the measurements were performed at room temperature under ambient atmosphere.

Results and Discussion

The synthetic routes of the three SMEs are shown in **Scheme 1**. TFTN-Br, FTFN-Br and FTTFN-Br possess similar structure, including a conjugated backbone and quaternary ammonium ions (-N(CH$_3$)$_3$$^+$). All of them were synthesized through

Pd(PPh$_3$)$_4$-catalyzed Stille coupling reaction. The quantitative quaternization is above 99% based on the disappearance of the signal of CH$_2$-Br in the ^{1}H NMR spectra at about δ= 3.26. The fluorene units are linked by thiophene and bithiophene in FTFN-Br and FTTFN-Br, respectively. However, two 5-octylthiophen units are connected to the 2, 7 position of fluorene unit in TFTN-Br. Due to the polar quaternary ammonium ions (-N(CH$_3$)$_3$$^+$), all SMEs have a good solubility in polar solvents, such as MeOH, DMSO and DMF.

The normalized Ultraviolet-visible (UV-vis) absorption spectra of TFTN-Br, FTFN-Br and FTTFN-Br in MeOH solution and their solid films on quartz substrates are shown in **Figure S2**, and the relevant data are listed in **Table S1** (SI). In solution, the absorption maximum (λ$_{abs}$) for TFTN-Br, FTFN-Br and FTTFN-Br located at 361 nm, 378 nm and 403 nm, respectively. Compared to their corresponding solutions, the films of the SMEs also showed the red-shifted λ$_{abs}$, indicating the strong intermolecular stacking in solid state.[28] In addition, both of the λ$_{abs}$ in solutions and films are red-shifted, due to the more ordered packing arrangement in the solid states. From the optical transmittance spectra of the SMEs coated on ITO (**Figure S3,** SI), due to the ultrathin thickness film of SMEs,[22] the ITO/SMEs substrates display a good transmittance (approximately same as bare ITO) in the visible light region. Therefore, the light-harvesting of active layer would not affected by the SMEs, and TFTN-Br, FTFN-Br and FTTFN-Br can be employed as electron transporting layer for inverted PSCs.

The energy levels of the SMEs were measured by the cyclic voltammetry (CV), as presented in **Figure S4** (SI). The highest occupied molecular orbital (HOMO) values and the lowest unoccupied molecular orbital (LUMO) values of the SMEs are obtained from the onsets of the oxidation potential (E$_{oneset/ox}$) and reduction potential (E$_{oneset/red}$), respectively.[29] The HOMO/LUMO values for TFTN-Br, FTFN-Br and FTTFN-Br are estimated to be -5.16/-2.60 eV, -5.34/-2.83 eV and -5.20/-3.00 eV,

respectively. Correspondingly, the electrochemical band gaps (E_g^{cv}) for TFTN-Br, FTFN-Br and FTTFN-Br are 2.56, 2.51 and 2.20 eV, respectively, which is consistent with the optical band gaps (E_g^{opt}) in **Table S1** (SI).

The density functional theory (DFT) computation was performed to give a preliminary insight into the geometric structures and dipolar property of the three SMEs by using the DFT B3LYP/6-31G (d) level with the Gaussian 09 suite of programs.[30] As shown in **Figure 1**, resulting from the electrostatic repulsion and steric hindrance, the two polar groups situated in the opposite side of the two fluorine unit backbone in FTFN-Br and FTTFN-Br, which subsequently lead to a low dipole moment. The different thiophene (T) bridge in FTFN-Br and FTTFN-Br caused a diverse dipole (11.4D in FTFN-Br and 9.4D in FTTFN-Br). Distinguishingly, the TFTN-Br only has one polar group in the backbone, whereby acquiring much stronger dipole moment (28.7D). The dipole moment in TFTN-Br is also stronger than the FFN-Br (10.6D), where the structure is similar to the well-known PFN-Br (**Figure S5,** SI). In addition, the structural variation also caused a distinctly different dihedral angle between the T unit and flanked benzene in the fluorine unit in the SMEs. Contrast to only one thiophene bridge in the FTFN-Br (the dihedral angles are 31.4° and -26.6°), two thiophene bridge make the backbone of FTTFN-Br more flexible and increase the distance between the two polar groups, which weaken the repulsion to a certain degree to obtain the smaller angles, -19.0°, 17.4° and -19.1°. Due to absence of the electrostatic repulsion from the opposite side of polar group, the dihedral angles in the TFTN-Br reduced to 24.3° and 23.4°.The various dipole moments in the SMEs would profoundly influence the interfacial properties, and the structural geometry would impact the interfacial morphology as well.[31]

The work function of ITO modified with TFTN-Br, FTFN-Br and FTTFN-Br was investigated by ultraviolet photoelectron spectroscopy (UPS). Here ZnO (sol-gel ZnO nanoparticles deposited on ITO substrate) was also presented for comparison.[19] The

high binding energy cutoffs (E_{cutoff}) of the SMEs and ZnO coated on ITO are shown in **Figure 2a**. The work function of bare ITO substrate is estimated to be 4.77 eV. Although ultrathin interlayer spin coated onto ITO, the E_{cutoff}, for ITO/SMEs has an obviously shift to higher energy. The shift of E_{vac} indicated that interfacial dipoles formed at the ITO/SMEs interfaces, which was equivalent to subtracting the work-function of ITO from the difference between the E_{vac} of SMEs film and the Fermi energy of ITO.[32, 33] Thus, the work function of ITO could be reduced by 0.35, 0.51, 0.74 and 0.89 eV with the introduction of ZnO, FTFN-Br, FTTFN-Br and TFTN-Br, respectively. The reduced work function would bring about a better energy alignment and electron extraction and collection.[34, 35] The energy level diagram of the photovoltaic cells is shown in **Figure 2b**. The variation of work function of the ITO after coated by FTFN-Br and FTTFN-Br is not as identical as our speculation from the DFT computation without consideration on conformation of SMEs onto ITO.

To probe the reason for variation of the work function of ITO modified by TFTN-Br, FTFN-Br and FTTFN-Br, X-ray photoelectron spectroscopy (XPS) was carried out to investigate the surface properties of ITO, ITO/ZnO, and ITO/SMEs. For the pure ITO, the In 3d XPS spectrum in **Figure 2c** has two peaks centered at 452.52 eV and 444.94 eV. Obviously, the In 3d peaks for ITO/ZnO, ITO/FTFN-Br, ITO/FTTFN-Br and ITO/TFTN-Br were shifted toward the lower binding energy by 0.51, 0.56, 0.73 and 0.80 eV, respectively, indicating the strong interaction between SMEs and ITO. Similar shift tendency is observed in the O 1s XPS spectra of ITO modified by ZnO and SMEs (**Figure 2d**). The shifts in the peaks of binding energies revealed the following: (i) the interaction between polar groups in SMEs and ITO surface existed and (ii) the backbone of SMEs influenced the chemical shifts.[36] From the shifts in the peaks of binding energies we can see that, ITO/TFTN-Br interface has the strongest interaction, while ITO/FTFN-Br has the lowest one, which is in accordance with the change in their work function.

To characterize the effect of SMEs on the surface of ITO, the water contact angles were measured for bare ITO, and for ITO modified with SMEs. The contact angles for bare ITO, TFTN-Br, FTFN-Br, and FTFN-Br were 49°, 74°, 45°, and 58°, respectively (**Figure S6**, SI). The contact angle of ITO modified with TFTN-Br was the largest, implying a more hydrophobic surface with conjugated backbone exposed to air. It is suspected that more hydrophobic backbones of the FTFN-Br and FTTFN-Br faced upward the surface.

To gain further insight into the surface of SMEs on ITO, a preferential interaction of SMEs onto ITO is proposed on the basis of the changes in XPS data, work function and water contact angles, which is shown in **Figure 3**. Due to the spontaneous orientation of SMEs, the ionic side chains tended to moved toward the hydrophilic ITO, whereas the hydrophobic aromatic backbone preferentially faced upward to the surface.[36-39] For TFTN-Br interlayer, all the ionic side chains oriented toward the ITO substrate, thereby developing the strongest interaction between ITO and TFTN-Br. However, according to the DFT computation, the ionic side chains of fluorene located at the both sides of the FTFN-Br and FTTFN-Br backbone, which would hinder them all to assemble onto ITO. Therefore, both FTFN-Br and FTTFN-Br get a relatively weaker interaction with the ITO versus TFTN-Br. Meanwhile, in order to ensure most of ionic side chains to anchor onto ITO substrate, the backones of FTFN-Br and FTTFN-Br are grabbed by ionic side chains toward to the ITO and have to adopt a flat plane (just like face-on conformation), which is quite different from the TFTN-Br presenting vertical plane on ITO. The difference in the conformation subsequently altered the dipole moments. As a result, TFTN-Br interlayer created the much stronger dipole moment (μ_D) at the interface than the FTFN-Br and FTTFN-Br, as shown in **Figure 3**. The strong and favorable dipole moment (μ_D) in TFTN-Br/ITO is correlated with the remarkable reduction of work function, which can lower the Schottky barrier and achieve a better energy alignment to facilitate the electron collection and transport from the active layer to ITO. Compared with FTFN-Br bearing one thiophene bridge,

FTTFN-Br with two thiophene bridge was more flexible, which is helpful for ionic side chains orienting toward the ITO and the backbone facing upward to the surface. The hydrophobic backone aggregated on the surface can be confirmed by the larger water contact angle of FTTFN-Br than that of FTFN-Br. Hence, the FTTFN-Br has the slightly stronger effect on ITO than FTFN-Br, which probably is the reason why the work functions of FTFN-Br and FTTFN-Br are different to those from the speculation of the DFT computation.

To evaluate the surface properties and morphology of TFTN-Br, FTFN-Br and FTTFN-Br. SMEs deposited on ITO were measured by atomic force microscopy (AFM) (**Figure 4a-d**). The standard ZnO surface was relatively smooth with a root-mean-square (RMS) roughness of 3.03 nm (**Figure 4a**), and the RMS roughness for FTTFN-Br (**Figure 4c**) and FTFN-Br (**Figure 4d**) are 3.04 nm and 4.67 nm, respectively. There is no obvious difference between FTFN-Br and FTTFN-Br in term of the surface RMS roughness for the similar conjugated backbones. However, due to the strongest interaction between TFTN-Br and ITO, TFTN-Br showed the roughest surface with a RMS of (**Figure 4b**) 7.25 nm.

The effect of the SMEs interfacial layer on the morphology of bulk-heterojunction (BHJ) active layer was also investigated. Although the interlayer is a thin film, the interlayer has an obvious influence on the morphology of active layer.[40, 41] The related AFM height images are shown in **Figure 4e-h**. The surface RMS roughness of P3HT:PC$_{61}$BM coated on FTTFN-Br and FTFN-Br (**Figure 4g** and **4h**) substrate is 4.96 nm and 5.49 nm, respectively. However, when use the TFTN-Br as the ETL, the active layer exhibits the highest RMS roughness of 6.82 nm (**Figure 4f**), which is primarily caused by the largest RMS roughness (7.25 nm) of the TFTN-Br substrate. Besides, the morphology change of the active layer on different SMEs surface caused by the different interlayers was further verified by transmission electron microscopy (TEM), as shown in **Figure 4i-l**. The TEM images of P3HT:PC$_{61}$BM films on

FTFN-Br, FTTFN-Br, and ZnO are similar. In comparison to P3HT:PC$_{61}$BM film deposited on FTFN-Br and FTTFN-Br, the blend film deposited on TFTN-Br achieve a more homogeneous morphology with the P3HT-rich phase and PCBM-rich phase with a small phase separation size,[42] which can facilitate the charge separation.

To investigate the influence of the backbones of SMEs on device performance, the inverted PSCs based on the SMEs were fabricated with the device architecture of ITO/SMEs/P3HT:PC$_{61}$BM/MoO$_3$/Ag. The SMEs were deposited on ITO as a cathode interface modification layer. **Figure 5a** shows the *J-V* curves of the devices based on P3HT:PC$_{61}$BM BHJ, which measured under AM 1.5 G solar irradiation and the device performance parameters are summarized in **Table 1**. All the SMEs interlayers were optimized at ultrathin thickness by optimized concentrations (0.5mg/mL) of their methanol solutions with same spin-coating speed. From **Figure 5** and **Table 1**, we can see that all of the devices with SMEs ETLs showed significantly improved PCE than the control device with ITO/MeOH (0.85%).[43] The PCE of the devices with SMEs is even comparable to that of standard device with ZnO ETL (a PCE of 3.0%), revealing that TFTN-Br, FTFN-Br and FTTFN-Br are effective materials for cathode interfacial modification. Especially, the PCE of the TFTN-Br based device achieved the highest PCE of 3.8%, with a V_{oc} of 0.616 V, a J_{sc} of 9.93 mA/cm^2 and a FF of 62.1%, giving 26% enhancement over the control device with ZnO as the cathode interlayer. However, devices with FTFN-Br and FTTFN-Br ETL show the relatively lower PCE of 3.1% and 3.5%, respectively. The overall enhanced parameters (PCE, V_{oc}, J_{sc} and FF) of SMEs-based devices are related to the achievement of better energy alignment, more compatible contact between each layer.[28]

Figure 5b reveals the *J-V* characteristics of the i-PSCs measured in the dark. In the range from -2 to 2 V, the dark current densities for the device with the SMEs are remarkably suppressed. There is an approximately 7× dark current density reduction upon the insertion of TFTN-Br. Therefore, the high photocurrent should also be

associated with the suppressed charge recombination induced by the enhanced interfacial contact at SMEs/active layer interface.[44, 45]

The influence of SMEs on the electron extraction was revealed by electron-only device measurements based on P3HT:PC$_{61}$BM blends using a structure of ITO/ETLs/P3HT:PC61BM/LiF/Al. The *J-V* characteristics were measured by the space charge limited current model (SCLC) according to the Mott-Gurney equation (details in the Supporting Information).[46-49] As shown in **Figure 5c**, the ZnO/P3HT:PC$_{61}$BM film gets the apparent electron mobility of 4.66×10^{-4} cm^{2}V^{-1}s^{-1}. Incorporation of these SMEs as the cathode buffer layer, the apparent electron mobility gradually increased to 8.95×10^{-4} cm^{2}V^{-1}s^{-1} for FTFN-Br, 1.29×10^{-3} cm^{2}V^{-1}s^{-1} for FTTFN-Br and 1.41×10^{-3} cm^{2}V^{-1}s^{-1} for TFTN-Br. The improved electron mobility contributed to increased J_{sc} and FF.

The incident photon-to-current efficiency (IPCE) values also agreed with the improved efficiency of the devices based on SMEs (**Figure 5d**). Obviously, with respect to the devices with FTFN-Br and ZnO, the TFTN-Br and FTTFN-Br based devices demonstrate significantly higher IPCE values in the wavelength range from 520-700 nm, in accordance with their higher J_{sc} values.

To research the influence of the SMEs on the device stability, the air stability of the unencapsulated i-PSCs with SMEs interlayer were periodically tested for 50 days (humidity, ~55%, ~25 °C) to monitor their long-term stability. As shown in **Figure S7** (SI), exposing to the air after 50 days, the PCE of the devices with TFTN-Br, FTFN-Br and FTTFN-Br can still retain approximately 66%, 68% and 63% of the original value, respectively, along with well-maintained J_{sc}, V_{oc}, and FF.[50] These results indicated that the stability of the device can be effectively improved by incorporation SMEs as cathode buffer layer.

Conclusions

In summary, three fluorene-based alcohol-soluble small molecular conjugated electrolytes, TFTN-Br, FTFN-Br and FTTFN-Br, bearing quaternary ammonium ion on side chains, were successfully designed and synthesized as cathode interlayer in P3HT:PC$_{61}$BM BHJ I-PSCs. Employing SMEs as interfacial layer effectively lowered the energy barrier, fine tuned the work function, and improved the inherent interface compatibility. Conspicuously, the device with TFTN-Br as ETL achieved a notable PCE of 3.8%. In comparison to devices with FTFN-Br (3.1%) and FTTFN-Br (3.5%), the devices of TFTN-Br show a higher J_{sc}, FF and V_{oc}, originating from the different conformation of their assembly onto the electrode caused by the sequence of polar group of SMEs, consequently impacting the dipole moment and interface morphology. Moreover, the better long-term stability in air indicates that the SMEs are a potential candidate for as the ETL. Our work boosts the understanding of the small molecular electrolytes cathode interlayer for i-PSCs and provides a new point of view to the development of novel cathode interlayer materials for i-PSCs.

ASSOCIATED CONTENT

Supporting Information

The details of general measurements and characterization; the UV-vis absorption spectra, cyclic voltammogram, optical transmittance spectra, and water contact angle measurement of the SMEs; the solubility of SMEs in methanol/chlorobenzene solution; the DFT calculated results of the FFN-Br; optical and electrochemical properties of the SMEs; stability test dates of the unencapsulated i-PSCs. This information is available free of charge via the Internet at http://pubs.rsc.org.

AUTHOR INFORMATION

Corresponding Author.

*E-mail: ywchen@ncu.edu.cn (Y. Chen)

Notes

Competing financial interests. The authors declare no competing financial interest.

Acknowledgements

References:

1.   B. C. Thompson and J. M. Frechet, *Angew. Chem., Int. Ed.*, 2008, **47**, 58-77.

2.   Y.-J. Cheng, S.-H. Yang and C.-S. Hsu, *Chem. Rev.*, 2009, **109**, 5868-5923.

3.   F. C. Krebs, T. Tromholt and M. Jørgensen, *Nanoscale*, 2010, **2**, 873-886.

4.   Z. He, B. Xiao, F. Liu, H. Wu, Y. Yang, S. Xiao, C. Wang, T. P. Russell and Y. Cao, *Nat. Photonics*, 2015, **9**, 174-179.

5.   Y. Liu, J. Zhao, Z. Li, C. Mu, W. Ma, H. Hu, K. Jiang, H. Lin, H. Ade and H. Yan, *Nat. commun.*, 2014, **5**.6293.

6.   X. Guo, N. Zhou, S. J. Lou, J. Smith, D. B. Tice, J. W. Hennek, R. P. Ortiz, J. T. L. Navarrete, S. Li and J. Strzalka, *Nat. Photonics*, 2013, **7**, 825-833.

7.   F. Zhang, X. Xu, W. Tang, J. Zhang, Z. Zhuo, J. Wang, J. Wang, Z. Xu and Y. Wang, *Sol. Energy Mater. Sol. Cells*, 2011, **95**, 1785-1799.

8.   A. K. K. Kyaw, D. H. Wang, V. Gupta, J. Zhang, S. Chand, G. C. Bazan and A. J. Heeger, *Adv. Mater.*, 2013, **25**, 2397-2402.

9.   K. Zhang, C. Zhong, S. Liu, C. Mu, Z. Li, H. Yan, F. Huang and Y. Cao, *ACS Appl. Mater. Interfaces*, 2014, **6**, 10429-10435.

10.   K. Kawano, R. Pacios, D. Poplavskyy, J. Nelson, D. D. Bradley and J. R. Durrant, *Sol. Energy Mater. Sol.Cells*, 2006, **90**, 3520-3530.

11.   M. De Jong, L. Van Ijzendoorn and M. De Voigt, *Appl. Phys. Lett.*, 2000, **77**, 2255-2257.

12.   S. V. Kesava, Z. Fei, A. D. Rimshaw, C. Wang, A. Hexemer, J. B. Asbury, M. Heeney and E. D. Gomez, *Adv. Energy Mater.*, 2014, **4**, 1400116.

13.   W. Ma, J. R. Tumbleston, L. Ye, C. Wang, J. Hou and H. Ade, *Adv. Mater.*, 2014, **26**, 4234-4241.

14.   J. A. Bartelt, J. D. Douglas, W. R. Mateker, A. E. Labban, C. J. Tassone, M. F. Toney, J. M. Fréchet, P. M. Beaujuge and M. D. McGehee, *Adv. Energy Mater.*, 2014, **4**, 1301733.

15.   Y. Yao, J. Hou, Z. Xu, G. Li and Y. Yang, *Adv. Funct. Mater.*, 2008, **18**, 1783-1789.

16.   H.-L. Yip and A. K.-Y. Jen, *Energy Environ. Sci.*, 2012, **5**, 5994-6011.

17. D. Ma, M. Lv, M. Lei, J. Zhu, H. Wang and X. Chen, *ACS Nano*, 2014, **8**, 1601-1608.

18. M.-F. Xu, Y.-J. Liao, F.-S. Zu, J. Liang, D.-X. Yuan, Z.-K. Wang and L.-S. Liao, *J. Mater. Chem. A*, 2014, **2**, 9400-9404.

19. Y. Sun, J. H. Seo, C. J. Takacs, J. Seifter and A. J. Heeger, *Adv. Mater.*, 2011, **23**, 1679-1683.

20. J. H. Seo, A. Gutacker, Y. Sun, H. Wu, F. Huang, Y. Cao, U. Scherf, A. J. Heeger and G. C. Bazan, *J. Am. Chem. Soc.*, 2011, **133**, 8416-8419.

21. A. Guerrero, S. Chambon, L. Hirsch and G. Garcia-Belmonte, *Adv. Funct. Mater.*, 2014, **24**, 6234-6240.

22. S. Liu, K. Zhang, J. Lu, J. Zhang, H.-L. Yip, F. Huang and Y. Cao, *J. Am. Chem. Soc.*, 2013, **135**, 15326-15329.

23. Y. Zhou, C. Fuentes-Hernandez, J. Shim, J. Meyer, A. J. Giordano, H. Li, P. Winget, T. Papadopoulos, H. Cheun and J. Kim, *Science*, 2012, **336**, 327-332.

24. A. K. K. Kyaw, D. H. Wang, D. Wynands, J. Zhang, T.-Q. Nguyen, G. C. Bazan and A. J. Heeger, *Nano Lett.*, 2013, **13**, 3796-3801.

25. K. Zilberberg, J. Meyer and T. Riedl, *J. Mater. Chem. C*, 2013, **1**, 4796-4815.

26. W. Zhang, Y. Wu, Q. Bao, F. Gao and J. Fang, *Adv. Energy Mater.*, 2014, **4**. 1400359.

27. S.-I. Na, S.-H. Oh, S.-S. Kim and D.-Y. Kim, *Org. Electron.*, 2009, **10**, 496-500.

28. Z. He, C. Zhong, X. Huang, W. Y. Wong, H. Wu, L. Chen, S. Su and Y. Cao, *Adv. Mater.*, 2011, **23**, 4636-4643.

29. J. Hou, Z. Tan, Y. Yan, Y. He, C. Yang and Y. Li, *J. Am. Chem. Soc.*, 2006, **128**, 4911-4916.

30. M. Frisch, G. Trucks, H. Schlegel, G. Scuseria, M. Robb, J. Cheeseman, G. Scalmani, V. Barone, B. Mennucci and G. Petersson, *Gaussian Inc., Wallingford, CT*, 2010.

31. I. Lange, S. Reiter, M. Pätzel, A. Zykov, A. Nefedov, J. Hildebrandt, S. Hecht, S. Kowarik, C. Wöll and G. Heimel, *Adv. Funct. Mater.*, 2014, **24**, 7014-7024.

32.   J. H. Seo and T.-Q. Nguyen, *J. Am. Chem. Soc.*, 2008, **130**, 10042-10043.

33.   J. H. Seo, R. Yang, J. Z. Brzezinski, B. Walker, G. C. Bazan and T. Q. Nguyen, *Adv. Mater.*, 2009, **21**, 1006-1011.

34.   J. Luo, H. Wu, C. He, A. Li, W. Yang and Y. Cao, *Appl. Phys. Lett.*, 2009, **95**, 043301.

35.   C. He, C. Zhong, H. Wu, R. Yang, W. Yang, F. Huang, G. C. Bazan and Y. Cao, *J. Mater. Chem.*, 2010, **20**, 2617-2622.

36.   R. Kang, S.-H. Oh and D.-Y. Kim, *ACS Appl. Mater. Interfaces*, 2014, **6**, 6227-6236.

37.   G. H. Jung, K.-G. Lim, T.-W. Lee and J.-L. Lee, *Sol. Energy Mater. Sol. Cells*, 2011, **95**, 1146-1150.

38.   B. H. Lee, I. H. Jung, H. Y. Woo, H. K. Shim, G. Kim and K. Lee, *Adv. Funct. Mater.*, 2014, **24**, 1100-1108.

39.   J. Park, R. Yang, C. V. Hoven, A. Garcia, D. A. Fischer, T.-Q. Nguyen, G. C. Bazan and D. M. DeLongchamp, *Adv. Mater.*, 2008, **20**, 2491-2496.

40.   X. Bulliard, S. G. Ihn, S. Yun, Y. Kim, D. Choi, J. Y. Choi, M. Kim, M. Sim, J. H. Park and W. Choi, *Adv. Funct. Mater.*, 2010, **20**, 4381-4387.

41.   C.-H. Hsieh, Y.-J. Cheng, P.-J. Li, C.-H. Chen, M. Dubosc, R.-M. Liang and C.-S. Hsu, *J. Amer. Chem. Soc.*, 2010, **132**, 4887-4893.

42.   X. Yang, J. Loos, S. C. Veenstra, W. J. Verhees, M. M. Wienk, J. M. Kroon, M. A. Michels and R. A. Janssen, *Nano Lett.*, 2005, **5**, 579-583.

43.   L. Hu, F. Wu, C. Li, A. Hu, X. Hu, Y. Zhang, L. Chen and Y. Chen, *Macromolecules*, 2015, **48**, 5578-5586.

44.   X. Gong, M. Tong, F. G. Brunetti, J. Seo, Y. Sun, D. Moses, F. Wudl and A. J. Heeger, *Adv. Mater.*, 2011, **23**, 2272-2277.

45.   S. R. Cowan, A. Roy and A. J. Heeger, *Phys. Rev. B*, 2010, **82**, 245207.

46.   G. Zhao, Y. He, Z. Xu, J. Hou, M. Zhang, J. Min, H. Y. Chen, M. Ye, Z. Hong and Y. Yang, *Adv. Funct. Mater.*, 2010, **20**, 1480-1487.

47.   Y. J. Cheng, C. H. Hsieh, P. J. Li and C. S. Hsu, *Adv. Funct. Mater.*, 2011, **21**, 1723-1732.

48.   C. Goh, R. J. Kline, M. D. McGehee, E. N. Kadnikova and J. M. Fréchet, *Appl. Phys. Lett.*, 2005, **86**, 122110.

49.   Y. Liu, X. Wan, F. Wang, J. Zhou, G. Long, J. Tian and Y. Chen, *Adv. Mater.*, 2011, **23**, 5387-5391.

50.   C. Xie, L. Chen and Y. Chen, *J. Phys. Chem. C*, 2013, **117**, 24804-24814.
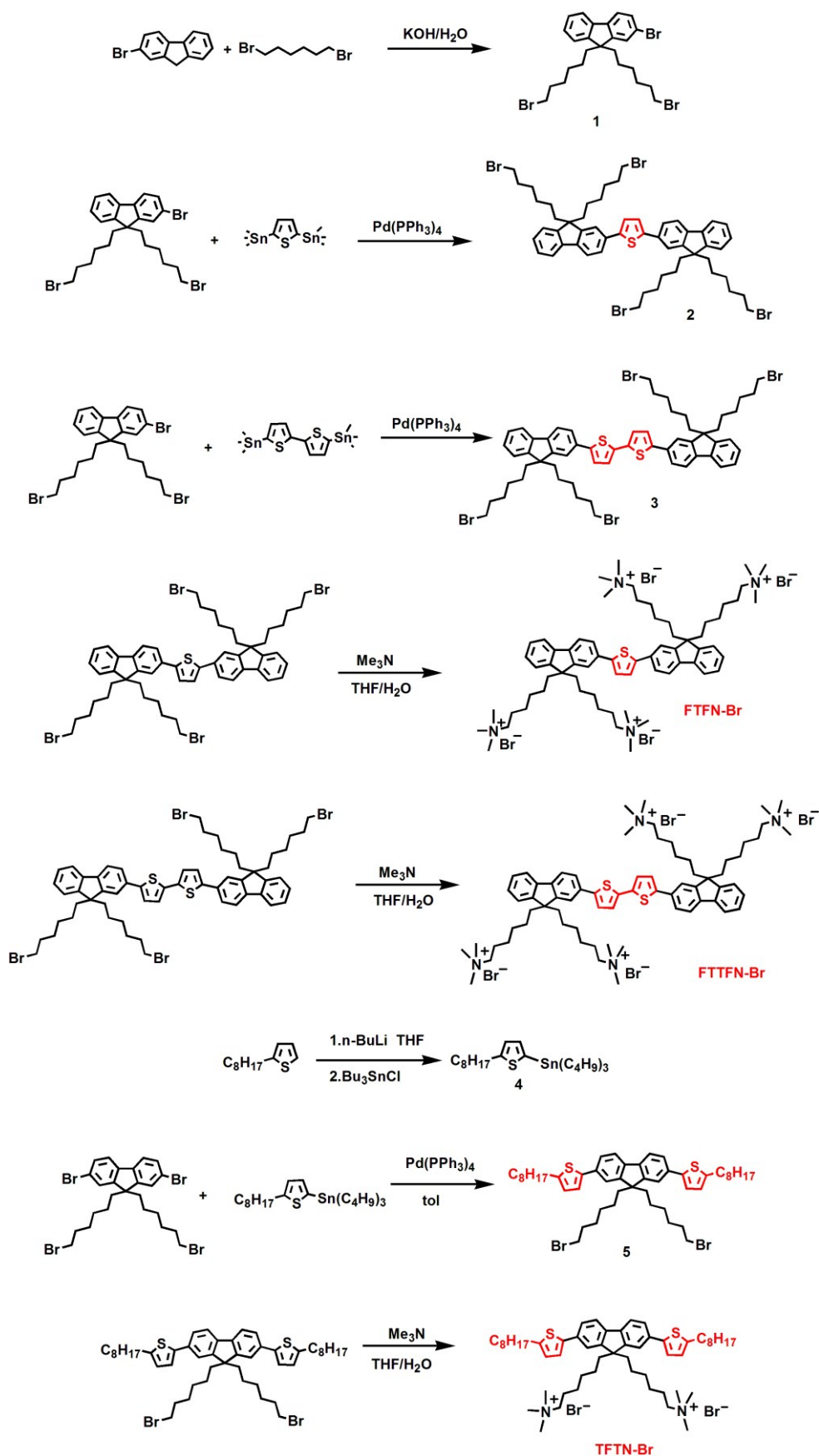
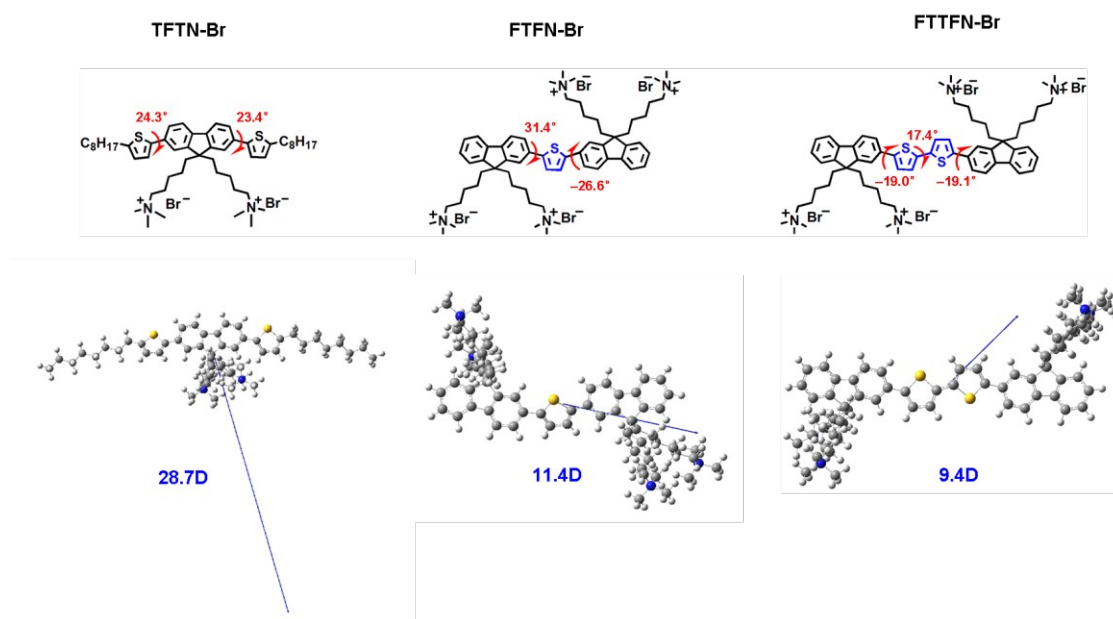**Scheme 1.** The synthetic routes for FTFN-Br, FTTFN-Br and TFTN-Br.

Figure 1. The calculated results of the geometric structures and dipolar properties of the SMEs
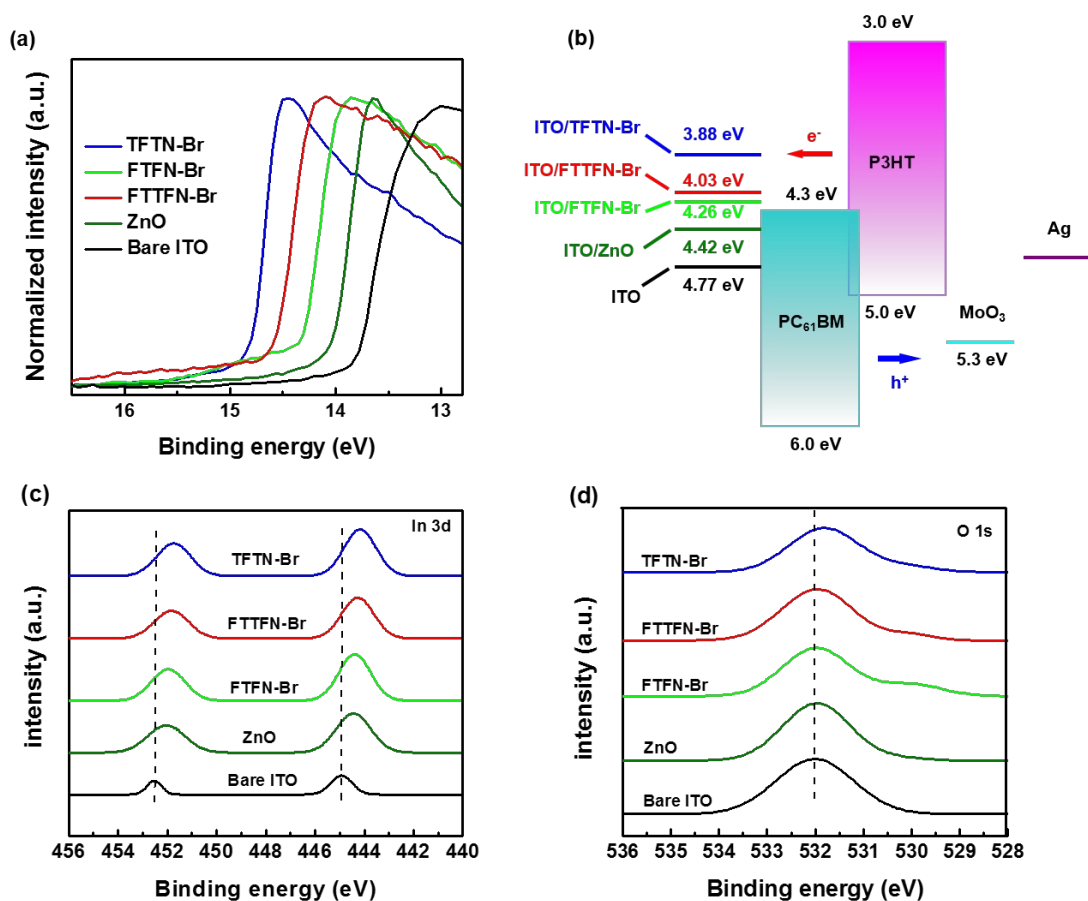
Figure 2. (a) The ultraviolet photoelectron spectroscopy (UPS) spectra of different SMEs spin-coated onto ITO, (b) Energy level diagram of the i-PSCs and electrical contacts of the cathodes with the LUMO level of $PC_{61}BM$. High-resolution X-ray photoelectron spectra of (c) In 3d; (d) O 1s on the surface of SMEs coated on ITO substrate
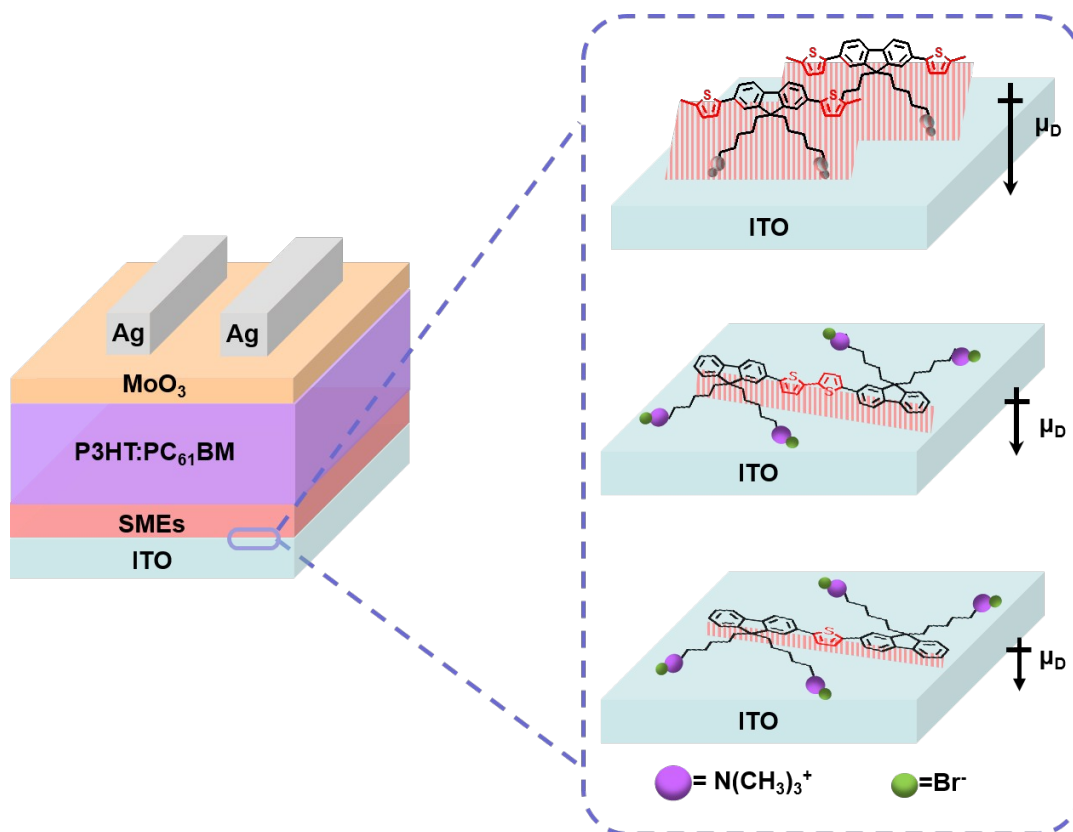
Figure 3. Schematic possible orientations of TFTN-Br, FTFN-Br and FTTFN-Br on ITO and device structure, comprising SMEs and MoO_3 as interfacial layers and a P3HT/PC_{61}BM active layer, sandwiched between the ITO cathode and Ag anode.
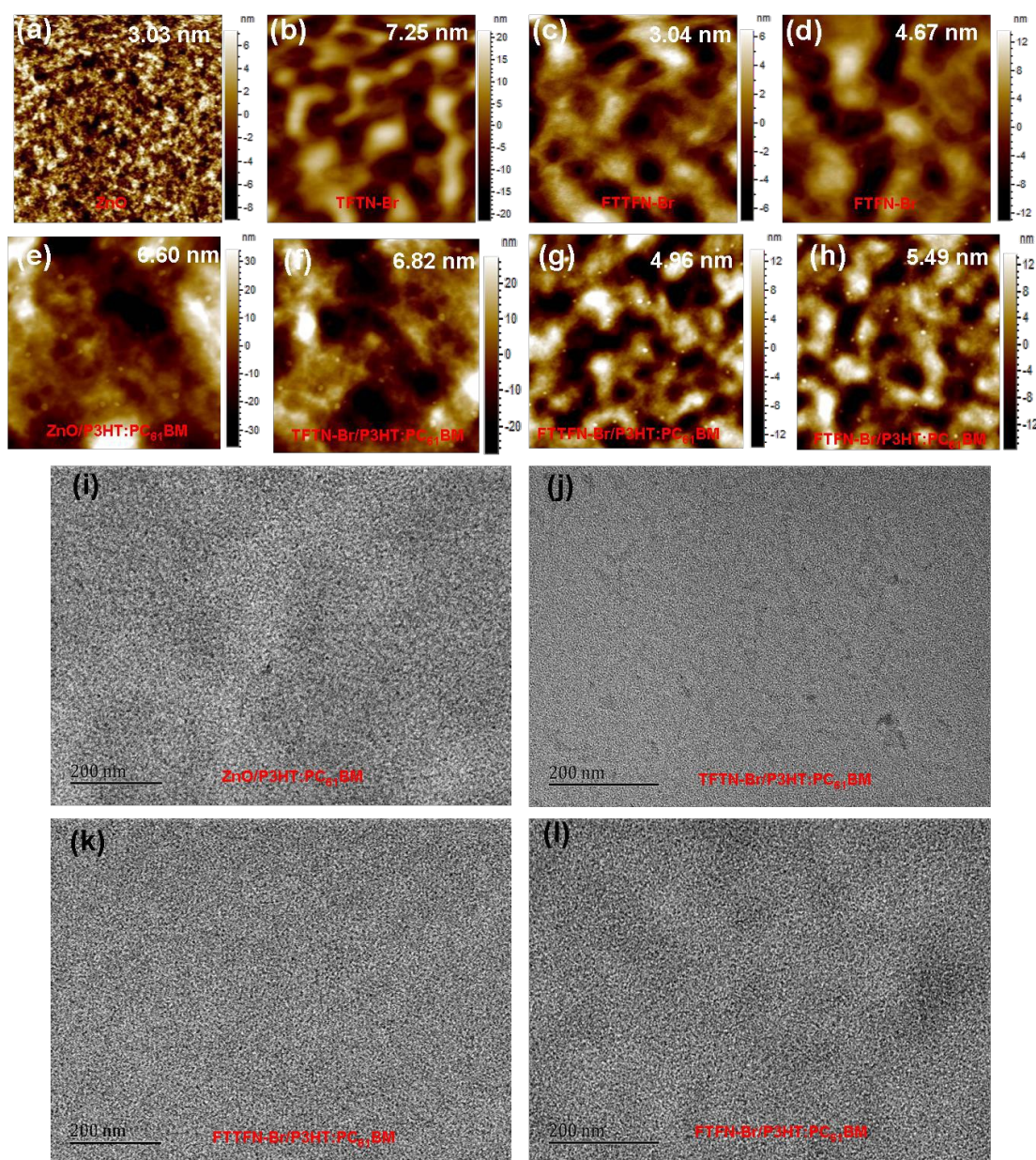
Figure 4. The atomic force microscopy (AFM) tapping mode height images of the surface of (a) Bare ZnO; (b) TFTN-Br; (c) FTTFN-Br; (d) FTFN-Br coated ITO glass; AFM height images of P3HT:PC$_{61}$BM films on top of the (e) bare ZnO; (f) TFTN-Br; (g) FTTFN-Br; (h) FTTFN-Br layer after thermal annealing at 150 °C for 10 min; (scan range:5μm×5μm;the scale bar on the right of each image relating the color to a height). Transmission electron microscopy (TEM) images of P3HT:PC$_{61}$BM films on top of the (i) ZnO; (j) TFTN-Br; (k) FTTFN-Br; (l) FTFN-Br layer.

Table 1. Summary of the photovoltaic performance of inverted P3HT:PC$_{61}$BM solar cells with various ETLs

Device configuration	J_{sc} (mA/cm^2)	V_{oc} (V)	FF (%)	PCE (%)	
ITO/MeOH [43]	7.63	0.371	30.2	0.85	/
ITO/ZnO	8.52	0.589	59.2	3.0 [a]	2.9±0.1 [b]
ITO/TFTN-Br	9.93	0.616	62.1	3.8 [a]	3.7±0.1 [b]
ITO/FTFN-Br	8.56	0.606	59.6	3.1 [a]	3.0±0.1 [b]
ITO/FTTFN-Br	9.30	0.607	61.2	3.5 [a]	3.4±0.1 [b]

All parameters were obtained from the [a] best devices except the [b] average PCE values that were obtained from the measurements using ten devices.
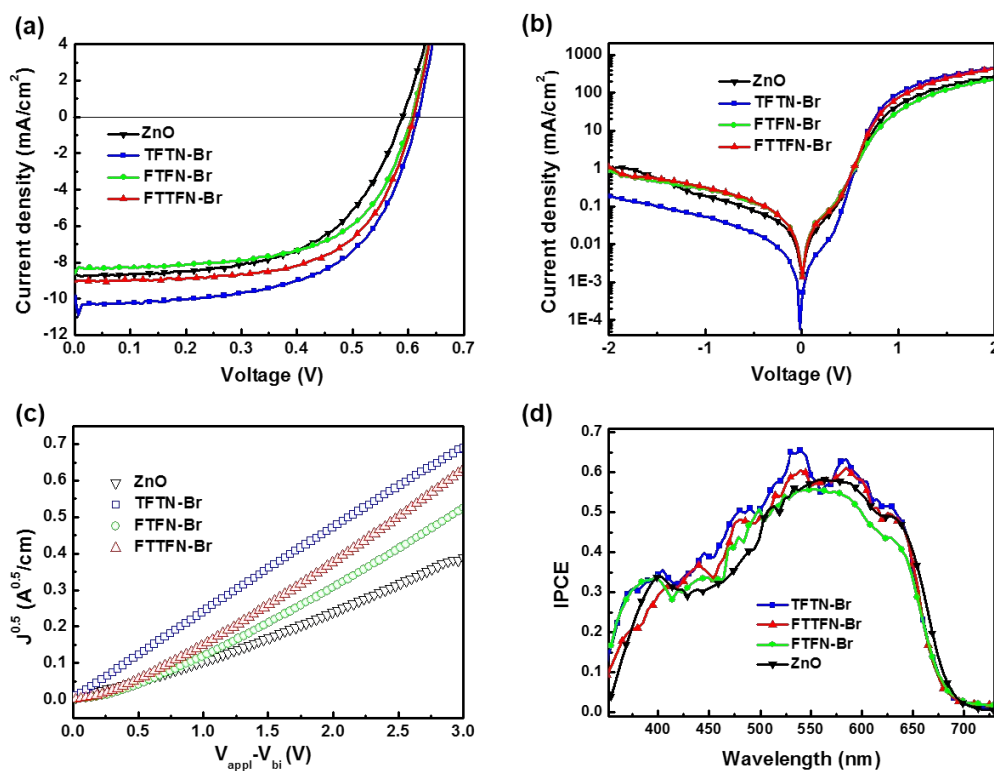
Figure 5. *J-V* characteristics (a) under AM 1.5G illumination at 100 mW cm^{-2} and (b) in the dark of the i-PSCs ITO/ETL/P3HT:PC$_{61}$BM/MoO$_3$/Ag with various ETLs, (c) *J*$^{0.5}$-V characteristics of electron-only with different cathode interfacial layers and (d) the corresponding EQE spectra of the device.

28

Table of Content

The joint sequence of polar group of small molecule electrolytes resulted in different conformations which impact the interface dipole moment.